

Pharmacology of a Plant Virus Immunotherapy Candidate for Peritoneal Metastatic Ovarian Cancer

Anthony O. Omole,[◆] Jessica Fernanda Affonso de Oliveira,[◆] Lucas Sutorus, and Nicole F. Steinmetz*



Cite This: *ACS Pharmacol. Transl. Sci.* 2024, 7, 445–455



Read Online

ACCESS |

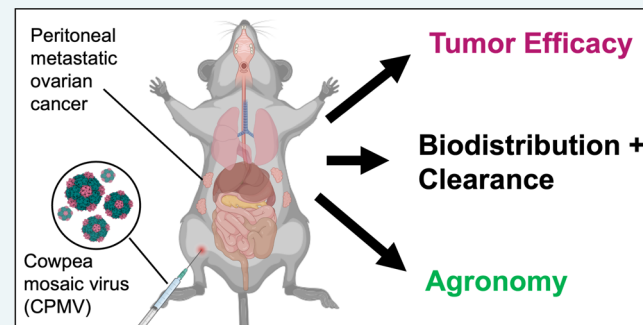
Metrics & More

Article Recommendations

Supporting Information

ABSTRACT: Due to the increasing incidence of cancer, there is a need to develop new platforms that can combat this disease. Cancer immunotherapy is a platform that takes advantage of the immune system to recognize and eradicate tumors and metastases. Our lab has identified a plant virus nanoparticle, cowpea mosaic virus (CPMV) as a promising approach for cancer immunotherapy. When administered intratumorally, CPMV relieves the immune system of tumor-induced immunosuppression and reprograms the tumor microenvironment into an activated state to launch systemic antitumor immunity. The efficacy of CPMV has been tested in many tumor models and in canine cancer patients with promising results: tumor shrinkage, systemic efficacy (abscopal effect), and immune memory to prevent recurrence. To translate this drug candidate from the bench to the clinic, studies that investigate the safety, pharmacology, and toxicity are needed. In this work, we describe the efficacy of CPMV against a metastatic ovarian tumor model and investigate the biodistribution of CPMV after single or repeated intraperitoneal administration in tumor-bearing and healthy mice. CPMV shows good retention in the tumor nodules and broad bioavailability with no apparent organ toxicity based on histopathology. Data indicate persistence of the viral RNA, which remains detectable 2 weeks post final administration, a phenomenon also observed with some mammalian viral infections. Lastly, while protein was not detected in stool or urine, RNA was shed through excretion from mice; however, there was no evidence that RNA was infectious to plants. Taken together, the data indicate that systemic administration results in broad bioavailability with no apparent toxicity. While RNA is shed from the subjects, data suggest agronomical safety. This data is consistent with prior reports and provides support for translational efforts.

KEYWORDS: *cancer immunotherapy, plant virus, cowpea mosaic virus, ovarian cancer, pharmacology*



Cancer nanotechnology refers to the application of nanotechnology to diagnose^{1,2} or treat cancer,³ and various nanoparticles are making headway through preclinical and clinical development.⁴ A key step in drug development is investigating pharmacology and safety. Our laboratory has focused on the development of plant viruses as a platform nanotechnology for human and veterinary health applications. One emerging drug candidate is the plant virus cowpea mosaic virus (CPMV), which is being developed as an intratumoral immunotherapy.⁵ Intratumoral CPMV remodels the tumor microenvironment (TME) and primes the immune-activated state; CPMV activates and recruits innate immune cells through pattern recognition (PRR), i.e., toll-like receptor (TLR) signaling.⁶ Innate immune cells kill tumor cells and become antigen-presenting cells, thus launching systemic and durable antitumor immunity through adaptive immune responses.⁷ CPMV efficacy is tumor agnostic in mouse tumor models and canine cancer patients—intratumoral CPMV immunotherapy reproducibly elicits promising efficacy, increases survival, and elicits durable immune memory protecting from recurrence.^{7–9}

CPMV is a 30 nm icosahedral plant picornavirus made up of 60 subunits of two coat proteins each: a 42 kDa large and 24 kDa small coat protein.¹⁰ CPMV primarily infects legumes and black-eyed peas through a common insect vector.¹¹ CPMV is immunogenic and generates B- and T-cell responses when administered in mice models.¹² Indeed, CPMV antibodies are also common in the human population, which indicates its prevalence and human exposure through the food chain or agricultural practices.¹¹

The pharmacology of CPMV and other plant viruses was investigated by us and others. Intravenously, CPMV is broadly bioavailable and persistent in tissues for days after a single administration.^{13,14} Intratumorally, CPMV resides within the tumor for days with minimal leaching into other organs.¹¹ In

Received: October 16, 2023

Revised: December 23, 2023

Accepted: December 27, 2023

Published: January 10, 2024



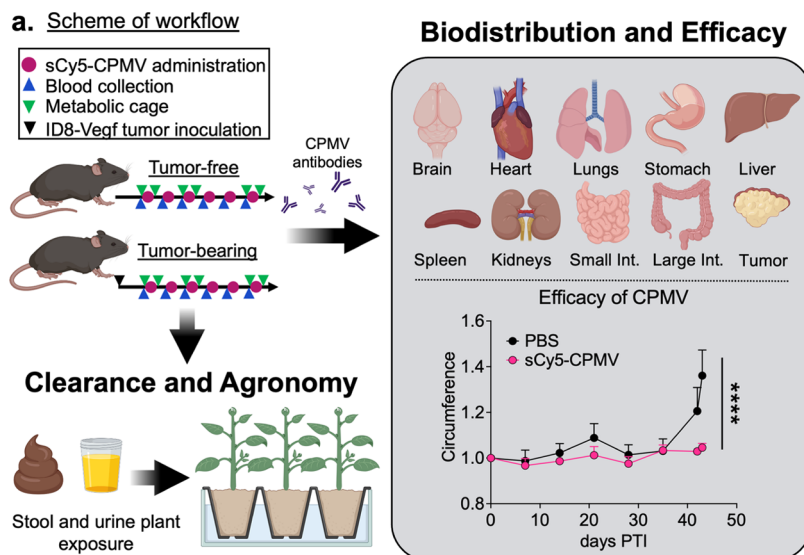


Figure 1. Schematic workflow. Biodistribution of CPMV is assessed after repeated administration. Clearance of CPMV is also monitored in stool and urine. Figure made in BioRender.

this study, we set out to investigate the pharmacology of CPMV when administered intraperitoneally in tumor-free and tumor-bearing mice; an intraperitoneal disseminated (metastatic) ovarian tumor model (ID8-Defb29-Vegf) was used.¹² In particular, we set up an assessment of biodistribution after single and repeat administration of CPMV (Figure 1). Organs were harvested 24 h and 2 weeks postadministration to assess acute and long-term pathological effects. In addition, we monitored the clearance/shedding of CPMV in urine and stool to address agronomical concerns, i.e., plant virus re-exposure to plants. In previous studies, we investigated the retention and pharmacology of CPMV in solid tumors;¹¹ here, we are interested in understanding the fate of CPMV after systemic administration (ip) against a metastatic tumor model. We also make preliminary investigations toward understanding viral RNA persistence and whether this may play a role in the CPMV's mechanism of action. Findings from this study add to the growing number of reports and development of CPMV for intratumoral immunotherapy.

RESULTS AND DISCUSSION

CPMV and sCy5-CPMV Synthesis and Characterization. CPMV was produced in black-eyed pea No. 5 (*Vigna unguiculata*) using previously established protocols.¹⁵ CPMV particles were fluorescently labeled with sulfo-cyanine 5 (sCy5) through NHS chemistry targeting exterior lysine residues^{16,17} (Figure 2a). UV-vis spectroscopy shows the typical spectrum of intact CPMV and sCy5-CPMV particles (Figure 2b) with an $A_{260:280}$ ratio of 1.7; data also confirms sCy5 conjugation, and analysis by the Beer–Lambert law indicates that ~40 sCy5 moieties were conjugated per CPMV particle.

Size exclusion chromatography showed pure and intact particles with an elution volume at ~10 mL on a Superose 6 Increase column (Figure 2c). There is no indication of aggregated or broken particles. All particle components—RNA and protein as well as sCy5 for the fluorescent conjugate—coelute from the column. This is consistent with dynamic light scattering showing a hydrodynamic diameter for CPMV and sCy5-CPMV at ~31–35 nm with a low polydispersity index

(PDI) of ~0.025 (Figure 2d). Denaturing gel electrophoresis shows size migration of the large coat protein (L-CP) and small coat protein (S-CP) at 42 and 24 kDa, respectively (Figure 2e). Under red light, fluorescently labeled coat proteins can be observed supporting covalent modification of the proteins. Native agarose gel also indicates comigration of proteins and RNA components shown through Coomassie blue staining of the protein and GelRed staining of the nucleic acids, respectively (Figure 2f). Under red light, fluorescently labeled sCy5-CPMV particles can be observed; this again confirms comigration of all components, i.e., intact CPMV particle formulations were obtained. Finally, transmission electron microscopy (TEM) imaging shows monodispersed and intact particles for both CPMV and sCy5-CPMV (Figure 2g).

Efficacy of CPMV against ip Disseminated Ovarian Cancer. For the tumor-bearing cohort, female CS7BL/6 mice were challenged with ID8-Defb29-Vegf ovarian cancer cells in the peritoneal space to mimic human disease, which often manifests with intraperitoneal (ip) metastases. This tumor model is highly aggressive and disseminates around the endothelial walls of the peritoneum.⁹ It is also slow growing with about 40 days before a significant difference between the treated and nontreated group. Seven days after tumor challenge, mice were treated ip with sCy5-CPMV and the others were injected with phosphate-buffered saline (PBS, vehicle-only control); treatment was given weekly for 6 weeks. The fold changes of the circumference and weight were monitored for both groups for over 40 days; an increase in abdominal circumference and body weight correlates to tumor burden and is a sign of ascites development (buildup of fluid in the abdomen). As previously demonstrated,^{9,12} CPMV therapy prevents ovarian tumor growth (Figure 3a,b). Mice receiving CPMV therapy (here, sCy5-CPMV) showed no signs of ascites formation. In stark contrast, PBS control mice had ascite formation and decreased mobility due to a significant increase in weight and circumference. ID8-Defb29-Vegf has been described as aggressive tumors disseminated in the ip space with an immunological “cold” phenotype; CPMV immunotherapy kickstarts the cancer-immunity cycle by recruitment

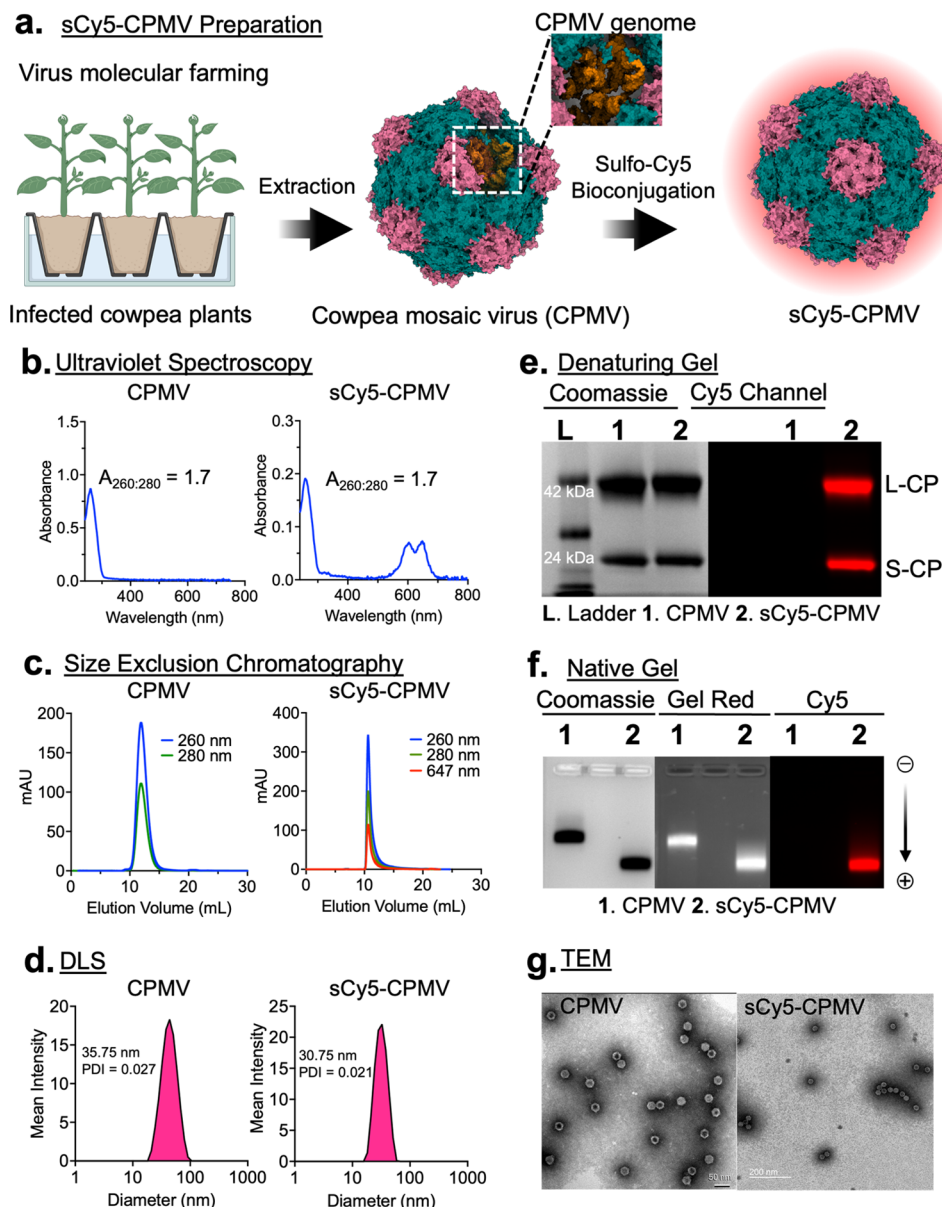


Figure 2. CPMV characterization: (a) CPMV is extracted from CPMV-infected plants and conjugated to sulfo-Cy5 through NHS chemistry. (b) UV-vis of CPMV and sCy5-CPMV show an $A_{260:280}$ ratio of ~1.7; sCy5-CPMV shows an absorbance peak at ~650 nm characteristic for the sCy5 dye. (c) Elution profile of CPMV and sCy5-CPMV from a Superose 6 Increase column is comparable; RNA ($A_{260\text{ nm}}$) and protein ($A_{280\text{ nm}}$) coelute and sCy5-CPMV being fluorescent ($A_{647\text{ nm}}$). (d) Dynamic light scattering (DLS) shows the hydrodynamic diameter of CPMV and sCy5-CPMV with a narrow polydispersity index (PDI). (e) Denaturing gel shows two coat proteins (S and L) and confirms conjugation of sCy5 in the case of sCy5-CPMV. (f) Native gel shows comigration of RNA (GelRed nucleic acid stain) and protein (Coomassie stain) for both CPMV and sCy5-CPMV and also confirms sCy5 conjugation to sCy5-CPMV (Cy5 channel). (g) Transmission electron microscopy (TEM) of native CPMV and sCy5-CPMV confirms uniform and unbroken particles. Panel (a) made in Biorender.

and activation of innate immune cells, such as neutrophils, dendritic cells (DCs), and natural killer (NK) cells.⁹ This immune priming leads to processing and enhanced presentation of tumor-associated and neoantigens, which primes cross-talks with the adaptive arm for T-cell and B-cell antitumor activities.^{5,9,18}

Biodistribution of sCy5-CPMV. Biodistribution of CPMV was assayed after multiple or single administrations, using healthy and tumor-bearing mice, and organs were harvested from mice cohorts after repeated sCy5-CPMV administration at 24 h and 2 weeks post final administration; the latter was included to assay whether clearance was achieved and to assay any potential chronic adverse effects. Quantification was

carried out through quantitative reverse transcription polymerase chain reaction (RT-PCR) to detect the viral genome or fluorescence measurements of the labeled capsid protein. High cycle thresholds in quantitative RT-PCR indicate low viral RNA detection, and vice versa. While the detection limit of the fluorescence measurements was less sensitive and also confounded by various tissues also having varying degrees of autofluorescence, the fluorescence detection of the labeled CPMV capsid protein allows us to assay the protein biodistribution relative to the RNA biodistribution.

It is of note that the metastatic ovarian tumor model grows aggressively along the epithelium; tumor nodules were collected and subjected to analysis: data shows significant

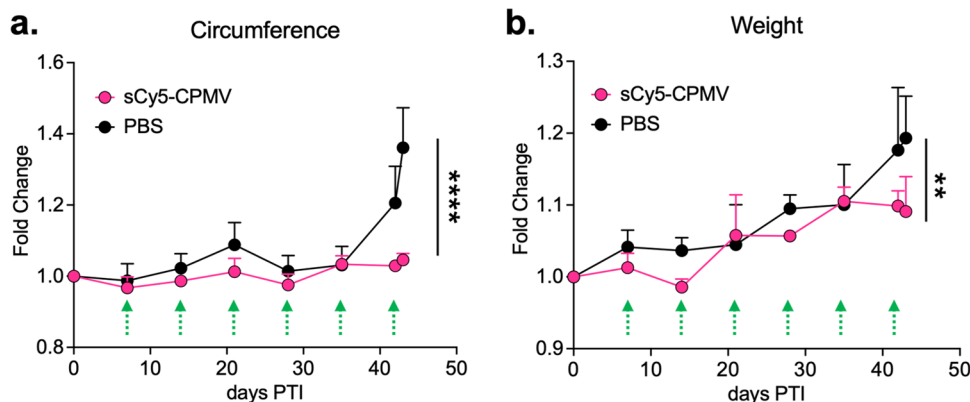


Figure 3. Efficacy of CPMV against peritoneal metastatic ovarian cancer. Female C57BL/6 mice, $n = 5$ per treatment group. Intraperitoneal tumor challenge: ID8-Defb29-Vegf ovarian tumor model. Treatment indicated by green dashed arrows: 100 μ g of sCy5-CPMV or PBS administered intraperitoneally, six times weekly. Significance calculated with two-way analysis of variance (ANOVA) (GraphPad Prism). **** $p < 0.0001$. ** $p = 0.0011$. (a) Mice circumference and treatment tumor curve. (b) Mice weight and treatment tumor curve.

accumulation of CPMV RNA and protein within the tumor nodules (Figures 4a–c and S1a). Overall, this data is consistent with what we observed in a mouse model of melanoma after intratumoral dosing of CPMV.¹¹ CPMV accumulates within the tumor tissue, and attesting to its nanoparticle character, it has good tumor retention. In the tumor-free cohort, 24 h after the final CPMV administration, CPMV RNA can be detected across all organs with minimal detection in the brain after repeated administration (Figure 4a). This is observed by the high cycle threshold average of 36 out of 40 cycles, which indicates the presence of low viral RNA in the brain. CPMV capsid proteins can also be detected across all organs (Figure 4c). This is consistent with previous reports showing broad biodistribution of CPMV after intravenous or intratumoral administration (here, dermal melanoma).^{11,13,14} Biodistribution in tumor-bearing and healthy mice was comparable, indicating that the disease does not affect biodistribution (Figure 4a–c). Because of this, we considered only healthy mice for subsequent experimental studies.

We compared biodistribution after single vs repeat administration to assay the effect of bioaccumulation with an increased number of dosing: based on RT-qPCR and fluorescence readouts (using a plate reader or an In Vivo Imaging Systems, IVIS), biodistribution was broad with organs testing positive, the only difference being that a lesser amount of CPMV was detected, not reaching the detection threshold for some organs (and this was more apparent for fluorescence readings) (Figures 4b,e and S1). While RT-qPCR did not show apparent differences, one notable difference was observed by IVIS and plate reader measurements, and that is the accumulation of CPMV in the lungs after repeated dosing (Figure 4b).

In prior work, using potato virus X (PVX), we made a similar observation. We found that biodistribution changes upon repeat systemic administration due to opsonization with plant virus-specific antibodies that are produced upon exposure.¹⁹ IgM antibody isotypes are the first to be induced after viral exposure and then undergoing a class switch to IgG.²⁰ Indeed, we detected anti-CPMV IgM and IgG antibodies in animals treated with CPMV (Figure S2). In particular, the presence of IgM may alter the biodistribution of (virus) nanoparticles; their pentavalent structure allows multivalent target binding to form immunocomplexes of increased size.^{19,20} The larger immunocomplexes have a

distinct pharmacology profile compared to their (virus) nanoparticle counterparts.²¹ These phenomena have been described for various nanoparticle systems, including PEGylated liposomes.²² Nevertheless, data indicates that this clearance through the lungs is not associated with acute or chronic lung histopathology (see Figure 6). Also, this work shows that CPMV exhibits potent efficacy against metastatic ovarian cancer after repeated treatment (Figure 3), and in fact, our prior work has shown that repeated doses are needed to achieve efficacy⁹ and—importantly—that the presence of anti-CPMV antibodies enhances the efficacy of CPMV against ovarian cancer: CPMV-IgG immunocomplexes are taken up by innate immune cells at faster rates compared to their “naked” counterparts; and it is this enhanced innate immune cell interaction that boosts the efficacy of intraperitoneal administrated CPMV against peritoneal metastatic cancer.¹²

Persistence of CPMV. Finally, we probed for the presence of CPMV across all organs 2 weeks after the final administration. CPMV RNA was detected across all organs, with the exception of the brain (Figure 5a). While previous reports suggested that CPMV was detectable after several days,^{13,14} no studies have investigated clearance after the 2-week time point. To gain insights into whether the RNA is retained in tissue as “free” RNA or packaged inside the CPMV capsid, we then performed a multiplexed immunofluorescence analysis to detect CPMV by labeling the capsid with an anti-CPMV antibody and RNA by fluorescence *in situ* hybridization (FISH). Imaging reveals that, indeed, CPMV RNA was detected in the liver, spleen, and kidney (organs involved in clearance); however, colocalization with the capsid was not apparent (Figure 5b–f). This data suggests that CPMV’s RNA has some tissue persistence—this is also observed for infectious viruses, such as SARS-CoV-2; the viral RNA can persist in tissues for weeks to months.²³

It may be worth investigating the impact of RNA persistence and prolonged immune activation and efficacy of the CPMV drug candidate. We have shown that eCPMV (empty CPMV: devoid of viral RNA) is an effective therapeutic; however, the presence of RNA in CPMV provides a more robust immune and antitumor response: CPMV RNA is recognized by TLR7 in the endosome.⁶ Studies have shown that the persistence of viral RNA from infectious viruses can lead to prolonged inflammation and immune response.²⁴ One could speculate, then, that the persistence of CPMV’s RNA may contribute to a

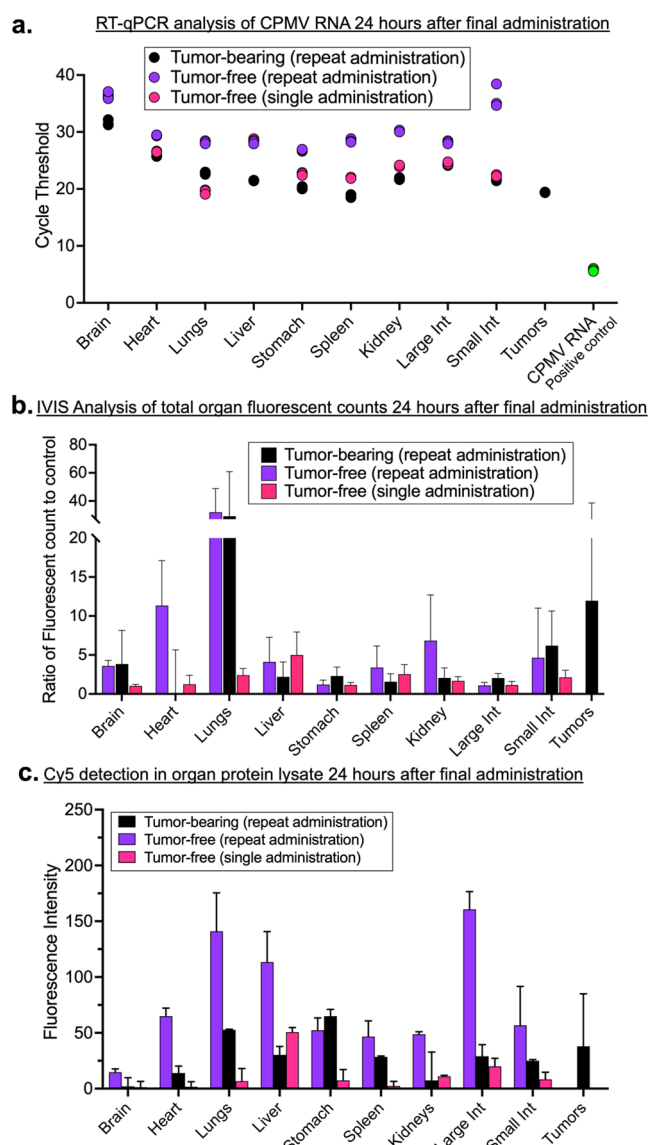


Figure 4. Biodistribution of CPMV across organs. (a) qPCR analysis of CPMV RNA in tumor-bearing mice. (b) In Vivo Imaging Systems (IVIS) ratiometric analysis of fluorescent counts after repeat administration in tumor-bearing mice, tumor-free mice, and tumor-free mice after single administration. (c) Fluorescence of sCy5-CPMV after repeat administration in tumor-bearing mice, tumor-free mice, and tumor-free mice after single administration. Tissues were collected 24 h post final administration; we also collected and analyzed tissues 2 weeks post final administration; this data is shown in Figure 5a.

sustained immune response. Further experiments are needed to explain the correlation.

Histopathology of CPMV. Next, we assayed whether CPMV presence and/or viral RNA persistence in tissues caused any toxicity, as determined by histopathology. We investigated whether CPMV after repeated dosing showed any signs of acute (harvested 24 h post final dose) or prolonged (harvested 2 weeks post final dose) organ toxicity. Organs were collected, sectioned, and H&E stained. There was no pathological finding in any organs, regardless of the time point of harvest (Figure 6a–e). This indicates that repeated administration of CPMV is nontoxic and nonpathological in short term or long term. This agrees with previous findings by

others, who investigated pathology after single dosing of CPMV;¹⁴ here, we focused on the pathology after repeat dosing and investigated acute and long-term effects. Overall, the literature reports are consistent, indicating that plant viruses are not causing toxicity in tissues, and similar data were reported for tomato bushy stunt virus (TBSV), potato virus X (PVX), and tobacco mosaic virus (TMV).^{25–27}

Shedding of CPMV after Administration and Agricultural Re-exposure. We investigated the shedding and clearance of CPMV particles to address potential agronomical concerns. Plant virus exposure in agriculture leads to high economic impacts and costs, and CPMV is infectious to various legumes.²⁸ And so, we investigated whether shedding of infectious particles would be of concern. We used metabolic cages to collect stool and urine from mice after the first, third, and sixth administration of sCy5-CPMV. CPMV RNA was detected through RT-PCR after the first and sixth administration in stool and urine (Figure 7a). This variability is something we also noted in a previous study and may reflect the labile nature of RNA.¹¹ Nevertheless, CPMV capsid protein could not be detected in stool and urine at any time point (Figure 7b), and also, this is consistent with our previous study.¹¹ To investigate whether stool and urine contain any infectious CPMV, we tested infection using black-eyed pea plants and mechanical inoculation of stool and urine samples that tested positive for CPMV RNA. Purified CPMV served as a positive control; infection was manifested with typical mosaic symptoms on the leaves (Figure 7c).²⁹ In stark contrast, infection was not apparent upon mechanical inoculation using urine or stool samples. This result was further validated by RT-PCR of homogenized leaf tissue, which showed that all samples were negative for infection with the exception of the positive control (Figure 7d). Thus, data indicates that while RNA is shed from animals, it is noninfectious toward plants. This is similar to what has been observed in infectious disease; viral RNA may be shed and hence can be used as an early warning system by sampling the sewage but is not a concern for reinfection.³⁰

CONCLUSIONS

CPMV shows promise as an immunotherapy for the treatment of women with ovarian cancer. The peritoneum and abdominal cavity are primary sites for metastatic ovarian cancer.^{31,32} Current efforts to tackle this disease include surgical debulking (also known as cytoreductive surgery); the aim of which is to reduce, not all but, visible tumors.³³ In addition to surgery, chemotherapeutic drugs are administered into the abdomen using a catheter, and this process is known as hyperthermic intraperitoneal chemotherapy (HIPEC).³³ While this is the standard-of-care for ovarian cancer (and other peritoneal metastatic cancers), intraperitoneal administration of chemotherapeutic drugs is underutilized in clinical settings for reasons, such as toxicities, patient discomfort, and infection of the area, even though it is effective.³⁴ Innovative strategies to address this include developing biodegradable implants to administer cancer drugs postsurgery or long-term postoperative care. Toward this goal, we have also shown that CPMV slow-release injectables can be effective as ip immunotherapy after single-dose administration.³⁵ CPMV is a potent intratumoral immunotherapy that can be used in the neoadjuvant setting prior to surgery or in combination with adjuvant chemotherapy.

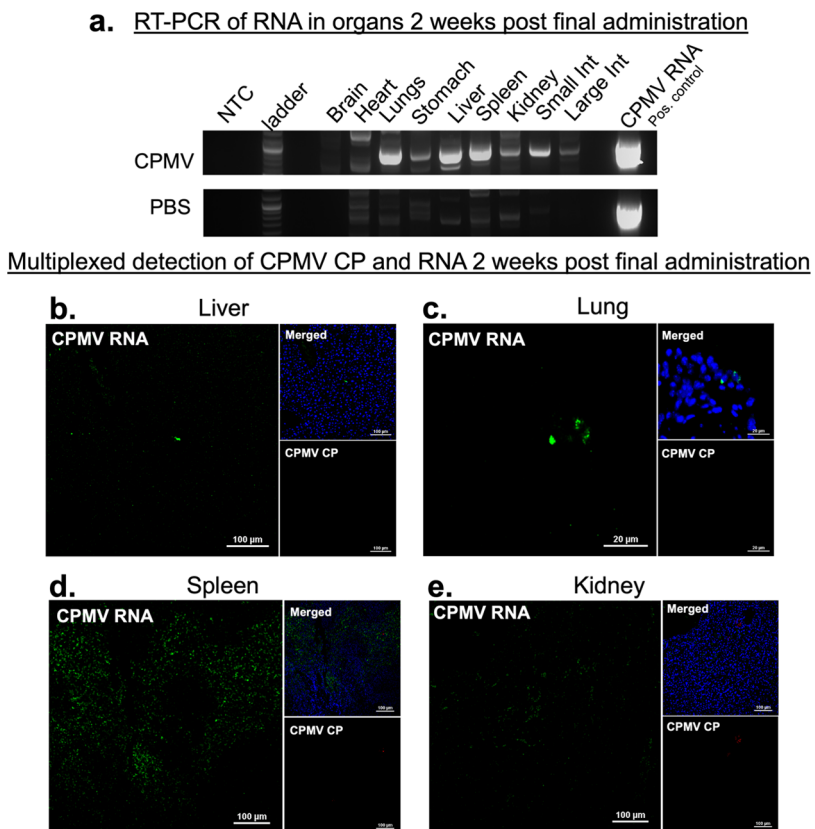


Figure 5. CPMV RNA (but not CP) persistence 2 weeks after final administration. (a) RT-PCR of CPMV RNA from organs 2 weeks after final repeated CPMV administration. (b–e) Multiplexed detection of CPMV RNA and CP in tissue slices. Green: CPMV RNA, red: CPMV CP, blue: DAPI. Images taken on confocal with 20× objective.

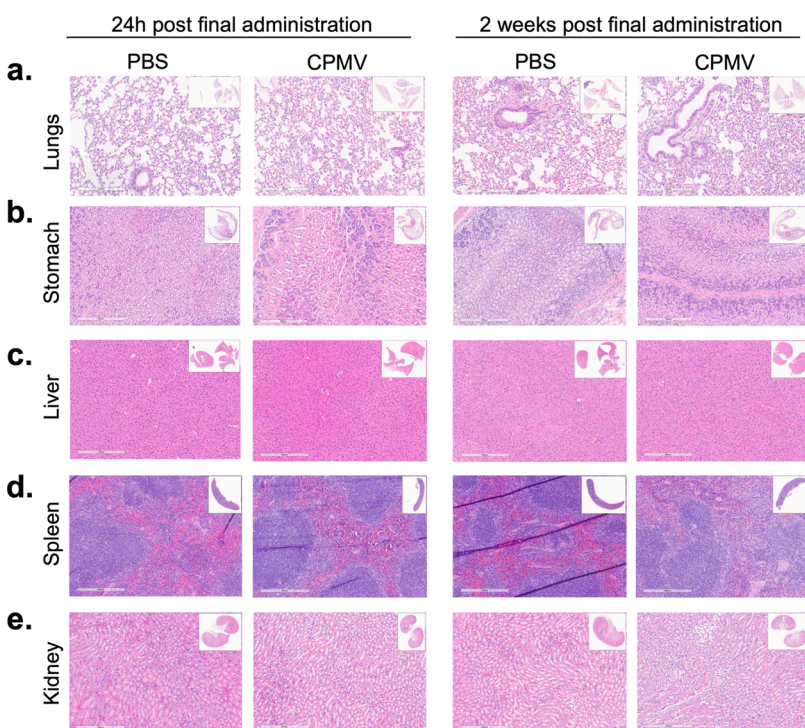


Figure 6. Histopathology of organs treated with CPMV. H&E staining of organ sections treated with CPMV and PBS 24 h and 2 weeks after final administration. Scale bar: 300 μm. Images analyzed with Aperio ImageScope.

As a step toward clinical translation, we investigated the pharmacology of CPMV after single and repeated dosing in

tumor-bearing and healthy mice. CPMV localizes within tumor nodules and is broadly bioavailable to organs. Acute or chronic

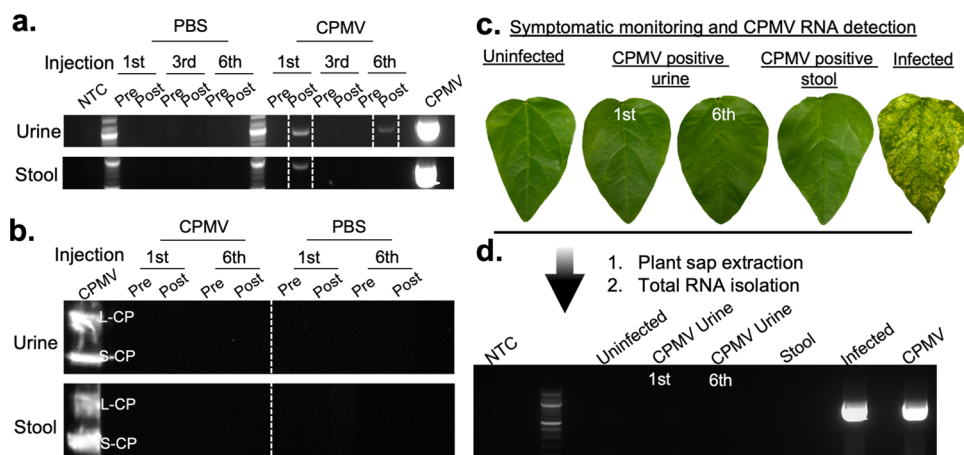


Figure 7. Shedding and clearance of CPMV RNA and virus exposure. (a) RT-PCR of CPMV RNA urine and stool after 1st, 3rd, and 6th injection. (b) Western blot against CPMV in urine and stool after 1st and 6th injection. (c) Symptomatic monitoring of CPMV infection on leaves exposed to CPMV-positive stool and urine. (d) RT-PCR of plant sap from leaves.

toxicity was not indicated based on histopathology, even though CPMV RNA was found to be persistent in reticuloendothelial system (RES) organs for at least 2 weeks postadministration. RNA shedding in urine was detected, but there is no evidence that infectious CPMV is cleared through stool or urine; this addresses agnomical concerns. These results are promising and bolster support for the clinical translation of CPMV.

MATERIALS AND METHODS

Cowpea Mosaic Virus Propagation and Preparation of sCy5-CPMV. CPMV was mechanically inoculated into black-eyed pea No. 5 plants (*V. unguiculata*) and purified as reported elsewhere.¹⁵ Cyanine-5 succinimide ester (NHS-sulfo-Cy5; Lumiprobe) was conjugated to CPMV's surface lysine residues by *N*-hydroxysuccinimide (NHS) chemistry as described in previous work.^{16,17} CPMV and sCy5-CPMV samples were stored at 4 °C until further characterization.

CPMV and sCy5-CPMV Characterization. UV-vis. A CPMV UV-vis Nanodrop 2000 (Thermo Fisher Scientific) was used to determine the degree of sCy5-labeling to CPMV; concentration of CPMV and sCy5-CPMV was calculated using the Beer–Lambert law of CPMV ($\epsilon_{\text{CPMV}} = 8.1 \text{ L/mol/cm}$ at 260 nm) and sCy5-CPMV ($\epsilon_{\text{sCy5}} = 270,000 \text{ L/mol/cm}$, at 647 nm).

Agarose Gel Electrophoresis. CPMV and sCy5-CPMV particles (10 mg) were loaded onto a 1.2% (w/v) agarose gel stained with GelRed (Gold Biotechnologies) in tris acetate ethylenediaminetetraacetic acid (TAE) buffer with 6× Gel Loading Purple dye (Biolabs). Gel was run at 120 V and 400 mA for 30 min and later imaged under a MultiFluor Red channel (607 nm excitation) to image the Cy5 dye, UV light to visualize the RNA, and further stained with Coomassie Brilliant Blue G-250 (0.25% w/v) and imaged under white light to detect the protein.

SDS-Gel Electrophoresis. Sodium dodecyl sulphate-polyacrylamide gel electrophoresis (SDS-PAGE) was used to confirm the covalent attachment of Cy5 to the CPMV coat proteins. Briefly, CPMV and sCy5-CPMV (10 mg) were mixed with 4× LDS running buffer (Life Technologies), denatured at 95 °C for 5 min, and loaded on precast NuPAGE 4–12% Bis Tris Protein Gel (Invitrogen). Electrophoresis was performed using 3-(*N*-morpholino)propanesulfonic acid (MOPS) buffer

(Thermo Fisher Scientific) for 40 min at 200 V. Gels were imaged under the MultiFluor Red channel (607 nm excitation; to image the Cy5 label) and then stained with GelCode Blue Safe protein stain and imaged under white light to detect the protein.

Dynamic Light Scattering (DLS). A Zetasizer Nano ZSP/ZenS600 (Malvern Panalytical) was used to assess the hydrodynamic diameter of CPMV and sCy5-CPMV (25 °C with three measurements per sample); the weighted mean of the intensity distribution was used to calculate the particle diameter.

Transmission Electron Microscopy (TEM). CPMV and sCy5-CPMV (0.1 mg/mL in deionized (DI) H₂O) were loaded onto Formvar carbon film-coated TEM supports with 400 mesh hexagonal copper grids (VWR International), which were rendered more hydrophilic using the PELCO easiGlow operating system. Grids were stained with 2% (w/v) uranyl acetate (Agar Scientific) and imaged by using an FEI TecnaiSpirit G2 BioTWIN TEM at 80 kV.

Size Exclusion Chromatography (SEC). An ÄKTA pure Fast Protein Liquid Chromatography system (GE Healthcare LifeSciences) was used to analyze CPMV and sCy5-CPMV (0.5 mg/mL) using a Superose6 Increase column size-exclusion column at a 0.5 mL/min flow rate. The elution profile was isocratic, and the UV detectors were fixed at 260 (nucleic acid), 280 nm (protein), and 647 nm (Cy5).

Tumor Model and Biodistribution Study. All animals used in this study were 7- to 8-week-old female C57BL/6 mice obtained from The Jackson Laboratory (Strain #000664). All animal experiments were carried out in accordance with the University of California San Diego's Institutional Animal Care and Use Committee (IACUC).

Syngeneic murine ovarian cancer cell lines, ID8-Defb29/Vegf-a, were cultured and maintained as previously reported.¹² A 2×10^6 live ID8-Defb29/Vegf-a cells were implanted orthotopically into mice by intraperitoneal (ip) injection (200 μL of sterile PBS). Mice were monitored weekly for signs of tumor burden, including weight, circumference, and abdominal distension. Seven days postcell ip inoculation, animals were injected with a single or multiple (6×/weekly) doses of CPMV or sCy5-CPMV ($n = 5$, 100 μg of particles in 200 μL of PBS, ip). PBS ($n = 5$, 200 μL) was used as controls for all treatment groups. The same set of healthy (tumor-free) mice were

injected with CPMV or sCy5-CPMV ($n = 5$, 100 μg of particles in 200 μL of PBS, ip). PBS ($n = 5$, 200 μL) was used as controls.

Ex Vivo Analysis. For ex vivo biodistribution studies, brain, heart, lungs, stomach, liver, spleen, kidneys, large and small intestines, and tumor were harvested 24 h or 2 weeks post final treatment and kept in RNAlater Stabilization Solution (Thermo Fisher Scientific) at -20°C until further analysis. sCy5-CPMV-treated mice organs were imaged using the IVIS Spectrum Imaging System (PerkinElmer Ltd.).

For fluorescence measurements, frozen organs from sCy5-CPMV-treated animals and controls were thawed, cut, weighed, and homogenized using PBS + 1× Protease Inhibitor Cocktail II (ab201116; 100 mg organ/mL) using a gentleMACS Dissociator (Miltenyi Biotec). Samples were centrifuged at 8000g for 5 min to remove tissue debris. Protein concentration was determined using Pierce BCA assay. 40 μg of supernatants was used to determine Cy5-specific fluorescence emissions ($\lambda_{\text{Ex}} = 633 \text{ nm}$ and $\lambda_{\text{Em}} = 665 \text{ nm}$) using an Infinite 200 Pro microplate reader and the software i-control (Tecan, Männedorf, Switzerland).

RNA Extraction. From Organs. Harvested organs were pooled, then cut, and homogenized using a gentleMACS Dissociator (Miltenyi Biotec). Total RNA extractions with lysates were performed with RNAqueous Total RNA Isolation Kit (cat. no. AM1912) according to the manufacturer's protocols. RNA integrity and concentration were assessed by UV-vis analysis.

From Stool and Urine. Stool and urine samples were collected with metabolic cage per IACUC guidelines. Stool was homogenized in a 1:1 volume ratio of 1× PBS (Corning, 21-040-CV) using a gentleMACS Dissociator (Miltenyi Biotec) and centrifuged at 4000g. The supernatant was isolated for total RNA extraction using the QIAamp Viral RNA mini kit (cat. no. 52904) according to manufacturer's protocols. Urine was centrifuged at 1500g for 10 min to pellet debris. Supernatant was isolated for total RNA extraction using the QIAamp Viral RNA mini kit (Cat# 52904) according to the manufacturer's protocols. RNA integrity and concentration were assessed by UV-vis analysis.

From Plant Sap. Leaves were pulverized under liquid nitrogen and resuspended in 4 mL of a cold 0.1 M KP, pH 7. The sample was centrifuged at 10,000g for 10 min to pellet debris. Supernatant was isolated for total RNA extraction using the QIAamp Viral RNA mini kit (Cat# 52904) according to the manufacturer's protocols. RNA integrity and concentration were assessed by UV-vis analysis.

Reverse Transcriptase Polymerase Chain Reaction (RT-PCR). Organs. Quantitative RT-PCR was performed using 25 ng of total RNA from samples with TaqMan Fast Virus 1-Step Master Mix (catalog no. 444432) according to the manufacturer's protocols. The experiments were performed on a BioRad CFX96 touch real-time PCR detection system in triplicate with 40 cycles. RNA probes were designed by Integrated DNA Technologies.

probe	5'-/56-FAM/TCGGGTTGT/ZEN/ TGTTTGATGTTGGCC/3IABkFQ/-3'
primer 1 (RV)	5'-CATGGAGTCTTGAGAGCAGATAG-3'
primer 2 (FW)	5'-ACAGCTACCACCAACATTCT-3'

Stool, Urine, Plant Sap. RT-PCR was performed using 100 ng of total RNA Invitrogen SuperScript IV one-step RT-PCR (Cat# 12594100) according to manufacturer's protocols.

Experiments were performed on a BioRad T100 PCR detection system, and PCR products were run on a 1.2% agarose gel (TAE) stained with GelRed. RNA probes were designed on Integrated DNA Technologies.

FW 5'-AGT GGT GAC CTT CCC AAA TAC-3'
RV 5'-GTC CAT CCC GAA ACA CAA ATA AC-3'

Western Blot. Pierce BCA Protein Assay (catalog no. 23277) was used to quantify total protein urine and stool samples according to the manufacturer's protocols. A total of 20 μg of total protein from urine and stool samples were separated on 4–12% SDS-PAGE precast gels in 1× MOPS buffer (40 min at 200 V), using SeeBlue Plus2 (Thermo Fisher Scientific) as a marker. Proteins were then electrotransferred onto a nitrocellulose membrane (Amersham Protran Premium 0.45 μm Nitrocellulose, GE Healthcare). Membranes were incubated with a rabbit anti-CPMV polyclonal antibody (1:1000; PAC 12273/12274), followed by horseradish peroxidase (HRP)-labeled goat antirabbit IgG (H + L) (1:5000; Fisher Scientific) and developed using Thermo Scientific Pierce ECL Western Blotting Substrate as described elsewhere.¹¹ Membranes were imaged using chemiluminescence on a ProteinSimple FluorChem R.

Antibody Titers and IgM Isotyping. Enzyme-linked immunosorbent assay (ELISA) was used to detect levels of CPMV-specific IgG in mice plasma after multiple CPMV or sCy5-CPMV administration. Blood samples were collected through retro-orbital bleeding before any ip procedure (i.e., prebleed) and then right before the second, third, fourth, fifth, and post 24 h after the last ip procedure (referred to as first, second, third, fourth, fifth, and sixth ip bleed). Serum was separated by centrifuging blood samples at 2000 rpm for 10 min and then stored at -20°C until being analyzed. ELISA assay was performed as described previously.¹¹ For CPMV-specific serum, IgM antibody titers were determined, following multiple administration of sCy5-CPMV in healthy and tumor-bearing animals (plasma from first, third, and sixth time points was analyzed). Plasma collected prior to the first sCy5-CPMV ip injection (prebleed) was used as naïve control, and the successive bleeds were compared to prebleed for changing antibody levels. We followed the ELISA protocol described above, except the secondary HRP-labeled goat antimouse antibodies specific for IgM (Abcam ab97230), diluted 1:5000 (100 μL /well, 1% (w/v) bovine serum albumin (BSA) in PBS).

Infectivity of CPMV from Stool and Urine in Plants. Metabolic cages were used to collect mice urine and stool from healthy mice ($n = 5$ per treatment group) and samples were collected for 4 h before CPMV and PBS ip injection and after 24 h after each treatment. Samples were processed and stored at -20°C until further analysis.³⁶ 7-day old black-eyed pea No. 5 plants were mechanically inoculated using carborundum with 20 μL of pooled stool and pooled urine supernatant samples. Twenty microliters of 0.1 mg/mL CPMV in 0.1 M KP buffer was used to mechanically inoculate leaves as a positive control. Leaves were photographed 14 days after infection, harvested, and stored at -80°C until RNA extraction.

Histological Examination. Organs were harvested and fixed in 10% neutral buffered formalin solution (Sigma, HT501128) overnight at a 10:1 volume ratio of fixation to tissue. Solution was changed to 70% ethanol and was submitted to UCSD Biorepository and Tissue Technology

Core for processing. Organs were fixed in paraffin before H&E staining. Histological examination was carried out by a core technician. The slides were read by a certified pathologist and the report was based on direct observation and references to the non-neoplastic Lesion Atlas from the National Toxicology Program and Mouse histology manuals.

Confocal Microscopy and Multiplexed Immunofluorescence and RNA In situ Hybridization. Organs fixed in paraffin mold were sliced and placed on a glass slide. Tissue slices were deparaffinized and rehydrated by baking at 60 °C and serial washing in xylene, 100% ethanol, 95%, 70%, 50%, and DI water for 10 min each. Heat-induced antigen retrieval was performed using 10 mM sodium citrate (0.05% tween) at 95 °C for 20 min and let to cool. Tissue slices were fixed in 8% paraformaldehyde (PFA) for 2 h at room temperature. To permeabilize, tissue slices were submerged in 70% ethanol overnight at 4 °C. Slices were blocked in 3% BSA in 1× PBS plus RNase inhibitor (New England Biolabs, M0307S) for 1 h and washed with 1× PBS for 5 min. For primary antibody incubation, Rabbit anti-CPMV (Pacific Immunology, PAC 12273/12274) antibodies were incubated on tissue slices at 2 µg/mL in 200 µL of 3% BSA in 1× PBS plus RNase inhibitor (New England Biolabs, M0307S) for 1 h and washed with 1× PBS for 5 min. For secondary antibody incubation, goat antirabbit Alexa Fluor 555 (Invitrogen) was incubated at 1:1000 in 200 µL of 3% BSA in 1× PBS plus RNase inhibitor (New England Biolabs, M0307S) for 1 h and washed with 1× PBS for 5 min. Slices were fixed again in 4% PFA in 1× PBS for 10 min at room temperature and then in 10% deionized formamide in 2× saline-sodium citrate (SSC) buffer for 10 min. Custom Stellaris probes (Quasar 647 dye) were designed against CPMV RNA probes using a Stellaris RNA FISH designer (Biosearch Technologies, LGC, Petaluma, CA). RNA hybridization was carried out at 37 °C using manufacturer's protocol available at www.biostoretech.com/stellarisprotocols. Slices were incubated in 10% deionized formamide in 2× SSC buffer for 10 min before glass slides were mounted on tissue slices with Fluoroshield with DAPI. Images were taken with 20× objective.

Statistical Analysis. Data were processed and analyzed using GraphPad Prism version 8.0.2 (GraphPad Software, San Diego, CA), unless otherwise indicated.

ASSOCIATED CONTENT

Supporting Information

The Supporting Information is available free of charge at <https://pubs.acs.org/doi/10.1021/acsppts.3c00285>.

Additional IVIS imaging data and antibody titers ([PDF](#))

AUTHOR INFORMATION

Corresponding Author

Nicole F. Steinmetz — Department of Nanoengineering, University of California, San Diego, La Jolla, California 92093-0021, United States; Shu and K.C. Chien and Peter Farrell Collaboratory, Institute for Materials Discovery and Design, and Center for Engineering in Cancer, Institute of Engineering Medicine, University of California, San Diego, La Jolla, California 92093, United States; Center for Nano-ImmunoEngineering, University of California, San Diego, La Jolla, California 92093-0403, United States; Moores Cancer Center, University of California, San Diego, La Jolla, California 92037, United States; Department of

Bioengineering, University of California, San Diego, La Jolla, California 92093-0412, United States; Department of Radiology, University of California, San Diego, La Jolla, California 92122, United States;  orcid.org/0000-0002-0130-0481; Email: nsteinmetz@ucsd.edu

Authors

Anthony O. Omole — Department of Nanoengineering, University of California, San Diego, La Jolla, California 92093-0021, United States; Shu and K.C. Chien and Peter Farrell Collaboratory, University of California, San Diego, La Jolla, California 92093, United States; Center for Nano-ImmunoEngineering, University of California, San Diego, La Jolla, California 92093-0403, United States; Moores Cancer Center, University of California, San Diego, La Jolla, California 92037, United States;  orcid.org/0000-0002-2323-2790

Jessica Fernanda Affonso de Oliveira — Department of Nanoengineering, University of California, San Diego, La Jolla, California 92093-0021, United States; Shu and K.C. Chien and Peter Farrell Collaboratory, University of California, San Diego, La Jolla, California 92093, United States; Center for Nano-ImmunoEngineering, University of California, San Diego, La Jolla, California 92093-0403, United States; Moores Cancer Center, University of California, San Diego, La Jolla, California 92037, United States

Lucas Sutorus — Department of Nanoengineering, University of California, San Diego, La Jolla, California 92093-0021, United States; Shu and K.C. Chien and Peter Farrell Collaboratory, University of California, San Diego, La Jolla, California 92093, United States; Center for Nano-ImmunoEngineering, University of California, San Diego, La Jolla, California 92093-0403, United States; Moores Cancer Center, University of California, San Diego, La Jolla, California 92037, United States

Complete contact information is available at:
<https://pubs.acs.org/10.1021/acsppts.3c00285>

Author Contributions

◆ A.O.O. and J.F.A.O. contributed equally. This manuscript was written through contributions of all authors. All authors have given approval to the final version of the manuscript.

Funding

This work was supported in part through NIH Grants R01 CA224605, R01 CA253615, and R01 CA274640 (to N.F.S.). N.F.S. acknowledges support through the Shaughnessy Family Fund for Nano-ImmunoEngineering (nanoIE) at UCSD as well as a UC San Diego Galvanizing Engineering in Medicine (GEM) Award. A.O.O. acknowledges support from San Diego Fellowship and the Alfred P. Sloan Foundation's Minority PhD (MPHD) Program (G-2020-14067).

Notes

The authors declare the following competing financial interest(s): N.F.S. is a co-founder of, has equity in, and has a financial interest with Mosaic ImmunoEngineering Inc. and is a co-founder and serves as manager of Pokometz Scientific LLC, under which she is a paid consultant to Mosaic ImmunoEngineering Inc., Flagship Labs 95 Inc., and Arana Biosciences Inc.

ACKNOWLEDGMENTS

The authors thank the University of California, San Diego—Cellular and Molecular Medicine Electron Microscopy Core (UCSD-CMM-EM Core, RRID: SCR_022039) for equipment access and technical assistance. The UCSD-CMM-EM Core is partly supported by the National Institutes of Health Award number S10OD023527. The authors thank the Kersi Pestonjamas and the UCSD Cancer Center Microscopy Shared Facility (Specialized Support Grant P30CA23100-28 and 2P30CA023100 by NCI) for providing equipment, services, and expertise to complete this work. Tissue Technology Shared Resource is supported by a National Cancer Institute Cancer Center Support Grant (CCSG Grant P30CA23100). Molecular graphics and analyses performed with UCSF Chimera, developed by the Resource for Biocomputing, Visualization, and Informatics at the University of California, San Francisco, with support from NIH P41-GM103311. Figures made with BioRender.

ABBREVIATIONS

CPMV, cowpea mosaic virus; IP, intraperitoneal; DAPI, 4',6-diamidino-2-phenylindole; SSC, saline-sodium citrate; HRP, horse radish peroxidase; KP, potassium phosphate; FISH, fluorescence *in situ* hybridization; PBS, phosphate-buffered saline; IVIS, In Vivo Imaging Systems; sCy5, sulfo-cyanine 5

REFERENCES

- (1) Kwon, E. J.; Dudani, J. S.; Bhatia, S. N. Ultrasensitive tumour-penetrating nanosensors of protease activity. *Nat. Biomed. Eng.* **2017**, *1*, No. 0054, DOI: 10.1038/s41551-017-0054.
- (2) Yaari, Z.; Yang, Y.; Apfelbaum, E.; Cupo, C.; Settle, A. H.; Cullen, Q.; Cai, W.; Long Roche, K.; Levine, D. A.; Fleisher, M.; Ramanathan, L.; Zheng, M.; Jagota, A.; Heller, D. A. A perception-based nanosensor platform to detect cancer biomarkers. *Sci. Adv.* **2021**, *7* (47), No. eabj0852.
- (3) Wang-Bishop, L.; Kimmel, B. R.; Ngwa, V. M.; Madden, M. Z.; Baljon, J. J.; Florian, D. C.; Hanna, A.; Pastora, L. E.; Sheehy, T. L.; Kwiatkowski, A. J.; Wehbe, M.; Wen, X.; Becker, K. W.; Garland, K. M.; Schulman, J. A.; Shae, D.; Edwards, D.; Wolf, M. M.; Delapp, R.; Christov, P. P.; Beckermann, K. E.; Balko, J. M.; Rathmell, W. K.; Rathmell, J. C.; Chen, J.; Wilson, J. T. STING-activating nanoparticles normalize the vascular-immune interface to potentiate cancer immunotherapy. *Sci. Immunol.* **2023**, *8* (83), No. eadd1153.
- (4) Ptak, K.; Farrell, D.; Panaro, N. J.; Grodzinski, P.; Barker, A. D. The NCI Alliance for Nanotechnology in Cancer: achievement and path forward. *Wiley Interdiscip. Rev.: Nanomed. Nanobiotechnol.* **2010**, *2* (5), 450–460.
- (5) Lizotte, P. H.; Wen, A. M.; Sheen, M. R.; Fields, J.; Rojanasopondit, P.; Steinmetz, N. F.; Fiering, S. In situ vaccination with cowpea mosaic virus nanoparticles suppresses metastatic cancer. *Nat. Nanotechnol.* **2016**, *11* (3), 295–303.
- (6) Mao, C.; Beiss, V.; Fields, J.; Steinmetz, N. F.; Fiering, S. Cowpea mosaic virus stimulates antitumor immunity through recognition by multiple MYD88-dependent toll-like receptors. *Biomaterials* **2021**, *275*, No. 120914.
- (7) Mao, C.; Beiss, V.; Ho, G. W.; Fields, J.; Steinmetz, N. F.; Fiering, S. In situ vaccination with cowpea mosaic virus elicits systemic antitumor immunity and potentiates immune checkpoint blockade. *J. Immunother. Cancer* **2022**, *10* (12), No. e005834.
- (8) Alonso-Miguel, D.; Valdivia, G.; Guerrera, D.; Perez-Alenza, M. D.; Pantelyushin, S.; Alonso-Diez, A.; Beiss, V.; Fiering, S.; Steinmetz, N. F.; Suarez-Redondo, M.; Vom Berg, J.; Peña, L.; Arias-Pulido, H. Neoadjuvant *in situ* vaccination with cowpea mosaic virus as a novel therapy against canine inflammatory mammary cancer. *J. Immunother. Cancer* **2022**, *10* (3), No. e004044.
- (9) Wang, C.; Fiering, S. N.; Steinmetz, N. F. Cowpea Mosaic Virus Promotes Anti-Tumor Activity and Immune Memory in a Mouse Ovarian Tumor Model. *Adv. Ther.* **2019**, *2* (5), No. 1900003.
- (10) Hesketh, E. L.; Meshcheriakova, Y.; Dent, K. C.; Saxena, P.; Thompson, R. F.; Cockburn, J. J.; Lomonosoff, G. P.; Ranson, N. A. Mechanisms of assembly and genome packaging in an RNA virus revealed by high-resolution cryo-EM. *Nat. Commun.* **2015**, *6* (1), No. 10113.
- (11) Affonso de Oliveira, J. F.; Chan, S. K.; Omole, A. O.; Agrawal, V.; Steinmetz, N. F. In Vivo Fate of Cowpea Mosaic Virus *In Situ* Vaccine: Biodistribution and Clearance. *ACS Nano* **2022**, *16* (11), 18315–18328.
- (12) Shukla, S.; Wang, C.; Beiss, V.; Steinmetz, N. F. Antibody Response against Cowpea Mosaic Viral Nanoparticles Improves *In Situ* Vaccine Efficacy in Ovarian Cancer. *ACS Nano* **2020**, *14* (3), 2994–3003.
- (13) Rae, C. S.; Wei Khor, I.; Wang, Q.; Destito, G.; Gonzalez, M. J.; Singh, P.; Thomas, D. M.; Estrada, M. N.; Powell, E.; Finn, M. G.; Manchester, M. Systemic trafficking of plant virus nanoparticles in mice via the oral route. *Virology* **2005**, *343* (2), 224–235.
- (14) Singh, P.; Prasuhn, D.; Yeh, R. M.; Destito, G.; Rae, C. S.; Osborn, K.; Finn, M. G.; Manchester, M. Bio-distribution, toxicity and pathology of cowpea mosaic virus nanoparticles *in vivo*. *J. Controlled Release* **2007**, *120* (1–2), 41–50.
- (15) Wellink, J. Comovirus isolation and RNA extraction. *Methods Mol. Biol.* **1998**, *81*, 205–209.
- (16) Wang, Q.; Kaltgrad, E.; Lin, T.; Johnson, J. E.; Finn, M. G. Natural supramolecular building blocks. Wild-type cowpea mosaic virus. *Chem. Biol.* **2002**, *9* (7), 805–811.
- (17) Wen, A. M.; Infusino, M.; De Luca, A.; Kernan, D. L.; Czapar, A. E.; Strangi, G.; Steinmetz, N. F. Interface of physics and biology: engineering virus-based nanoparticles for biophotonics. *Bioconjugate Chem.* **2015**, *26* (1), 51–62.
- (18) Shukla, S.; Wang, C.; Beiss, V.; Cai, H.; Washington, T.; Murray, A. A.; Gong, X.; Zhao, Z.; Masarapu, H.; Zlotnick, A.; Fiering, S.; Steinmetz, N. F. The unique potency of Cowpea mosaic virus (CPMV) *in situ* cancer vaccine. *Biomater. Sci.* **2020**, *8* (19), 5489–5503.
- (19) Shukla, S.; Dorand, R. D.; Myers, J. T.; Woods, S. E.; Gulati, N. M.; Stewart, P. L.; Commandeur, U.; Huang, A. Y.; Steinmetz, N. F. Multiple Administrations of Viral Nanoparticles Alter *In Vivo* Behavior—Insights from Intravital Microscopy. *ACS Biomater. Sci. Eng.* **2016**, *2* (5), 829–837.
- (20) Gong, S.; Ruprecht, R. M. Immunoglobulin M: An Ancient Antiviral Weapon - Rediscovered. *Front. Immunol.* **2020**, *11*, No. 1943, DOI: 10.3389/fimmu.2020.01943.
- (21) Li, S.-D.; Huang, L. Pharmacokinetics and Biodistribution of Nanoparticles. *Mol. Pharmaceutics* **2008**, *5* (4), 496–504.
- (22) El Sayed, M. M.; Shimizu, T.; Abu Lila, A. S.; Elsadek, N. E.; Emam, S. E.; Alaaeldin, E.; Kamal, A.; Sarhan, H. A.; Ando, H.; Ishima, Y.; Ishida, T. A mouse model for studying the effect of blood anti-PEG IgMs levels on the *in vivo* fate of PEGylated liposomes. *Int. J. Pharm.* **2022**, *615*, No. 121539.
- (23) Chen, B.; Julg, B.; Mohandas, S.; Bradfute, S. B.; RECOVER Mechanistic Pathways Task Force. Viral persistence, reactivation, and mechanisms of long COVID. *eLife* **2023**, *12*, No. e86015, DOI: 10.7554/eLife.86015.
- (24) Griffin, D. E. Why does viral RNA sometimes persist after recovery from acute infections? *PLoS Biol.* **2022**, *20* (6), No. e3001687.
- (25) Blandino, A.; Lico, C.; Baschieri, S.; Barberini, L.; Cirotto, C.; Blasi, P.; Santi, L. In vitro and *in vivo* toxicity evaluation of plant virus nanocarriers. *Colloids Surf., B* **2015**, *129*, 130–136.
- (26) Lico, C.; Giardullo, P.; Mancuso, M.; Benvenuto, E.; Santi, L.; Baschieri, S. A biodistribution study of two differently shaped plant virus nanoparticles reveals new peculiar traits. *Colloids Surf., B* **2016**, *148*, 431–439.
- (27) Bruckman, M. A.; Randolph, L. N.; VanMeter, A.; Hern, S.; Shoffstall, A. J.; Taurog, R. E.; Steinmetz, N. F. Biodistribution,

pharmacokinetics, and blood compatibility of native and PEGylated tobacco mosaic virus nano-rods and -spheres in mice. *Virology* **2014**, *449*, 163–173.

(28) Jones, R. A. C. Global Plant Virus Disease Pandemics and Epidemics. *Plants* **2021**, *10* (2), No. 233, DOI: 10.3390/plants10020233.

(29) Lomonossoff, G. P. Cowpea Mosaic Virus. In *Encyclopedia of Virology*; Elsevier, 2008; pp 569–574.

(30) Cerrada-Romero, C.; Berastegui-Cabrera, J.; Camacho-Martinez, P.; Goikoetxea-Aguirre, J.; Perez-Palacios, P.; Santibanez, S.; Jose Blanco-Vidal, M.; Valiente, A.; Alba, J.; Rodriguez-Alvarez, R.; Pascual, A.; Oteo, J. A.; Miguel Cisneros, J.; Pachon, J.; Casas-Flecha, I.; Cordero, E.; Pozo, F.; Sanchez-Cespedes, J. Excretion and viability of SARS-CoV-2 in feces and its association with the clinical outcome of COVID-19. *Sci. Rep.* **2022**, *12* (1), No. 7397.

(31) Halkia, E.; Spiliotis, J.; Sugarbaker, P. Diagnosis and management of peritoneal metastases from ovarian cancer. *Gastroenterol. Res. Pract.* **2012**, *2012*, No. 541842.

(32) van Baal, J. O. A. M.; van Noorden, C. J. F.; Nieuwland, R.; Van de Vijver, K. K.; Sturk, A.; van Driel, W. J.; Kenter, G. G.; Lok, C. A. R. Development of Peritoneal Carcinomatosis in Epithelial Ovarian Cancer: A Review. *J. Histochem. Cytochem.* **2018**, *66* (2), 67–83.

(33) Huo, Y. R.; Richards, A.; Liauw, W.; Morris, D. L. Hyperthermic intraperitoneal chemotherapy (HIPEC) and cytoreductive surgery (CRS) in ovarian cancer: A systematic review and meta-analysis. *Eur. J. Surg. Oncol.* **2015**, *41* (12), 1578–1589.

(34) Wright, A. A.; Cronin, A.; Milne, D. E.; Bookman, M. A.; Burger, R. A.; Cohn, D. E.; Cristea, M. C.; Griggs, J. J.; Keating, N. L.; Levenback, C. F.; Mantia-Smaldone, G.; Matulonis, U. A.; Meyer, L. A.; Niland, J. C.; Weeks, J. C.; O’Malley, D. M. Use and Effectiveness of Intraperitoneal Chemotherapy for Treatment of Ovarian Cancer. *J. Clin. Oncol.* **2015**, *33* (26), 2841–2847.

(35) Czapar, A. E.; Tiu, B. D. B.; Veliz, F. A.; Pokorski, J. K.; Steinmetz, N. F. Slow-Release Formulation of Cowpea Mosaic Virus for In Situ Vaccine Delivery to Treat Ovarian Cancer. *Adv. Sci.* **2018**, *5* (5), No. 1700991, DOI: 10.1002/advs.201700991.

(36) Kim, J. M.; Kim, H. M.; Lee, E. J.; Jo, H. J.; Yoon, Y.; Lee, N. J.; Son, J.; Lee, Y. J.; Kim, M. S.; Lee, Y. P.; Chae, S. J.; Park, K. R.; Cho, S. R.; Park, S.; Kim, S. J.; Wang, E.; Woo, S.; Lim, A.; Park, S. J.; Jang, J.; Chung, Y. S.; Chin, B. S.; Lee, J. S.; Lim, D.; Han, M. G.; Yoo, C. K. Detection and Isolation of SARS-CoV-2 in Serum, Urine, and Stool Specimens of COVID-19 Patients from the Republic of Korea. *Osong Public Health Res. Perspect.* **2020**, *11* (3), 112–117.